de Haas–van Alphen and Shubnikov–de Haas oscillations in RAgSb$_2$ (R=Y, La-Nd, Sm)

K. D. Myers, S. L. Bud'ko, V. P. Antropov, B. N. Harmon, and P. C. Canfield
Ames Laboratory and Department of Physics and Astronomy, Iowa State University, Ames, Iowa 50011

A. H. Lacerda
National High Field Laboratory, Los Alamos Facility, Los Alamos National Laboratory, Los Alamos, New Mexico 87545
(Received 28 May 1999)

de Haas–van Alphen and Shubnikov–de Haas oscillations have been used to study the Fermi surface of the simple tetragonal RAgSb$_2$ series of compounds with R=Y, La-Nd, and Sm. The high quality of the flux-grown single crystals, coupled with very small extremal cross sections of Fermi surface, allow the observation of quantum oscillations at modest fields ($H<30$ kG) and high temperatures (up to 25 K in SmAgSb$_2$). For $H\|c$, the effective masses, determined from the temperature dependence of the amplitudes, are quite small, typically between 0.07 and $0.5m_0$. The topology of the Fermi surface was determined from the angular dependence of the frequencies for R=Y, La, and Sm. In SmAgSb$_2$, antiferromagnetic ordering below 8.8 K is shown to dramatically alter the Fermi surface. For LaAgSb$_2$ and CeAgSb$_2$, the effect of applied hydrostatic pressure on the frequencies was also studied. Finally, the experimental data were compared to the Fermi surface calculated within the tight-binding linear muffin-tin orbital approximation. Overall, the calculated electronic structure was found to be consistent with the experimental data. [S0163-1829(99)09443-6]

I. INTRODUCTION

Recent measurements of the primitive tetragonal RAgSb$_2$ series of compounds have shown these materials to manifest rich and complex magnetic and transport properties.[1,2] These compounds crystallize in the primitive tetragonal ZrCuSi$_2$ structure ($P4/nmm$, No. 129), which consists of Sb-RSb-Ag-RSb-Sb layers with the rare earth in a position with tetragonal point symmetry (4mm). The crystal electric-field splitting of the Hund's rule ground state constrains the local magnetic moments to lie within the basal plane for most of the compounds. Additional anisotropy is also observed within the basal plane of DyAgSb$_2$.[2] In this compound, up to 11 different metamagnetic states exist, depending on the magnitude and direction of the applied field within the basal plane. The magnetic ordering temperatures range from below 2 K in TmAgSb$_2$ to 12.8 K in GdAgSb$_2$ and approximately scale with the de Gennes factor which indicates the exchange interaction between the local moments is indirect, via the Ruderman-Kittel-Kasuya-Yosida (RKKY) interaction.

Although the magnetic properties of the RAgSb$_2$ compounds have been characterized, little is currently known of the electronic structure. The transverse magnetoresistance of the RAgSb$_2$ compounds was previously shown[1] to be very large [$\Delta\rho(H=55\,\mathrm{kG})/\rho_0\approx 60$ in SmAgSb$_2$] and strongly anisotropic with a much greater response for the field applied parallel to the c axis than within the basal plane. The magnetoresistance in all compounds is nearly linear and no signs of saturation were observed in any of the compounds in applied fields up to 55 kG. Furthermore, the transverse magnetoresistance of LaAgSb$_2$ does not saturate up to 180 kG, which suggests that the RAgSb$_2$ compounds are low carrier density compensated metals. The detailed study of de Haas–van Alphen (dHvA) and Shubnikov–de Haas (SdH) oscillations presented here allows for a more thorough characterization of the Fermi surface of these compounds.

After a brief presentation of the experimental methods specific to the investigation of the quantum oscillations, data will be presented on the frequency spectra of de Haas–van Alphen and Shubnikov–de Haas oscillations in the RAgSb$_2$ series for R=Y, La, Pr, Nd, and Sm. The calculated Fermi surface will be used to discuss the origin of the various observed frequencies and their angular dependence. Finally, the temperature dependence of the oscillations will be used as a probe of the effects of magnetic order on the electronic structure of the compounds.

II. EXPERIMENTAL DETAILS

High quality single crystals of the RAgSb$_2$ series of compounds with R=Y, La, Pr, Nd, and Sm were flux grown[3] from an initial composition of $R_{0.045}$Ag$_{0.091}$Sb$_{0.864}$. This Sb-rich self-flux was chosen because of its low melting temperature and because it introduces no new elements into the melt. The additional silver content also helps to preclude formation of RSb$_2$, an interesting[4] but currently unwanted second phase. The constituent elements were placed in alumina crucibles and sealed in quartz under a partial argon pressure. The starting materials were heated to 1200 °C, and then cooled to 670 °C over 120 h. Removal of the flux revealed platelike crystals with dimensions up to 1×1×0.5 cm and masses of nearly 1 g. The c axis was perpendicular to the plate.

As previously reported,[1,2] powder x-ray diffraction and single-crystal x-ray diffraction were used to verify the crystal structure and determine the purity of the single crystals. The lattice parameters were consistent with previous reports[5–7] and no site deficiencies were observed. Extremely weak peaks corresponding to a small amount of residual Sb on the surface of the single crystals were observed in the powder-diffraction data.

 ©1999 The American Physical Society

The magnetization measurements were performed in a Quantum Design superconducting quantum interference device (SQUID) magnetometer up to 55 kG, with the samples manually aligned. A specially modified horizontal rotor was used to obtain the angular dependent data for the $SmAgSb_2$. Samples were carefully chosen on the basis of size and geometry and to minimize the effects of any residual flux on the surface. Angular dependent torque measurements were also performed in a Quantum Design Physical Property Measurements System (PPMS) up to 90 kG, using the torque magnetometer[8] and horizontal rotator options. Uncertainty in the angular position is estimated to be less than one degree. Due to the larger magnetic moments and strong anisotropies in $NdAgSb_2$ and $PrAgSb_2$,[1] these samples were unsuitable for measurements in the PPMS.

Resistivity measurements used the temperature-field environment of the magnetometer, with a Linear Research LR-400 AC resistance bridge. A wire saw was used to cut the crystals into suitable geometry for resistance measurements with typical dimensions of 1×1×5 mm. Contacts were attached with Epotek-H20E silver epoxy, yielding typical contact resistances of about 1 Ω.

Measurements of Shubnikov–de Haas effect under pressure in $LaAgSb_2$ and $CeAgSb_2$ were performed in an Oxford Instruments cryostat with a variable-temperature insert and 180 kG superconducting magnet in NHMFL-Los Alamos, using nonmagnetic Be-Cu piston-cylinder clamp-type pressure cell with a light mineral oil as the pressure media. Pressure at room temperature was measured *in situ* with a manganin resistive manometer. The pressure values at liquid-helium temperatures were then calculated using previous calibration for this cell.[9]

In all cases, the quantum oscillations were separated from the background magnetization or magnetoresistance by subtracting either a power law or a polynomial fit of the $M(H)$, $\tau(H)$, or $\rho(H)$ data. Microcal Origin was used to create the fast Fourier transforms (FFT) of the data, after the background was subtracted. When possible, the data were acquired with varying applied field intervals such that the intervals in H^{-1} were constant. When this is not possible, such as the measurements in the PPMS and the SdH measurements under pressure, an interpolation routine was used to generate constant H^{-1} intervals. The number of points used in interpolation method was adjusted to check for any artifacts appearing in the FFT.

The temperature dependence of the amplitude of oscillations in the magnetization was used to determine the cyclotron effective masses. For an orbit with frequency F the amplitude of the oscillation in the magnetization M is given by the Lifshitz-Kosevitch (LK) equation:[10]

$$M = -2.602\times 10^{-6}\left(\frac{2\pi}{HA''}\right)^{1/2} \times \frac{GFT\exp(-\alpha px/H)}{p^{3/2}\sinh(-\alpha pT/H)}\sin\left[\left(\frac{2\pi pF}{H}\right)-\frac{1}{2}\pm\frac{\pi}{4}\right],$$

where $\alpha = 1.47\,(\mathrm{m}/m_0)\times 10^5$ G/K, A'' is the second derivative of the cross sectional area of the Fermi surface with respect to wave vector along the direction of the applied field, G is the reduction factor arising from electron spin, p is the number of the harmonic of the oscillation, and x is the Dingle temperature.

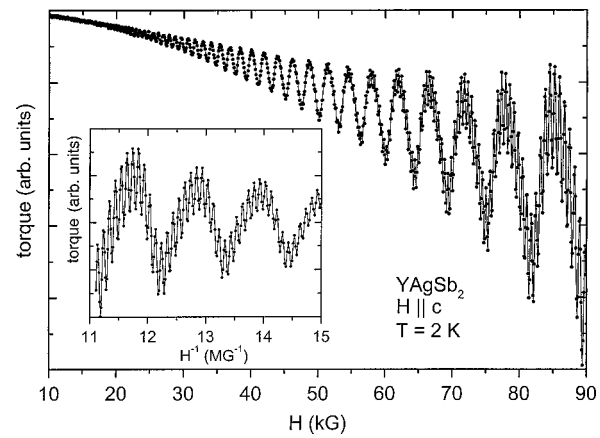

FIG. 1. Torque as a function of applied field in $YAgSb_2$ at 2 K for $H\|c$. Inset: detailed view of the torque as a function of H^{-1} between 60 and 90 kG.

In several cases, oscillations are observed in the magnetization data that are not present in the torque magnetometer data. The torque due to quantum oscillations is sensitive to the anisotropy of the Fermi surface and is given by

$$T = \frac{-1}{F}\frac{dF}{d\theta}MHV,$$

where M is given by the LK expression above, θ is the angle of the applied field, and V is the volume of the sample. Since the torque is dependent on the derivative of the frequency with respect to the angle of the applied field, some oscillations may not be observed if the field is applied along high-symmetry directions or if the Fermi surface is spherical.

III. DATA AND EXPERIMENTAL ANALYSIS

$YAgSb_2$

Exceptionally clear oscillations are observed in the applied field-dependent torque of $YAgSb_2$ at 2 K, shown in Fig. 1. The inset to Fig. 1 provides a detailed view of the torque as a function of inverse field between 66.7 and 90 kOe. The two frequencies easily observed in the torque data correspond to strong peaks in the Fourier spectra [Fig. 2(a)] at 0.86 MG (β) and 10.04 MG (δ). Smaller signals are also present at frequencies of 0.65 MG (α) and 1.82 MG (γ).

The temperature dependence of the amplitudes (A) of these frequencies, shown in the inset of Fig. 2(a), may be used to determine the effective mass of the orbits via the LK formula, described above. From the slope of $\ln(A/T)$ plotted as a function of temperature, the effective masses were found to be $m_\beta = 0.16(2)m_0$, $m_\gamma = 0.28(2)m_0$, and $m_\delta = 0.46(2)m_0$, where m_0 is the bare electron mass.

An estimate of the topology of the Fermi surface may be obtained from the angular dependence of the frequencies of each quantum oscillation. As seen in Fig. 2(b), the frequencies of the α and γ orbits do not diverge with increasing angle and may be fit to the angular dependence of the cross section of an ellipsoid (dotted lines) with c/a ratios of 4.3 for both orbits. On the other hand, the frequencies of the β and

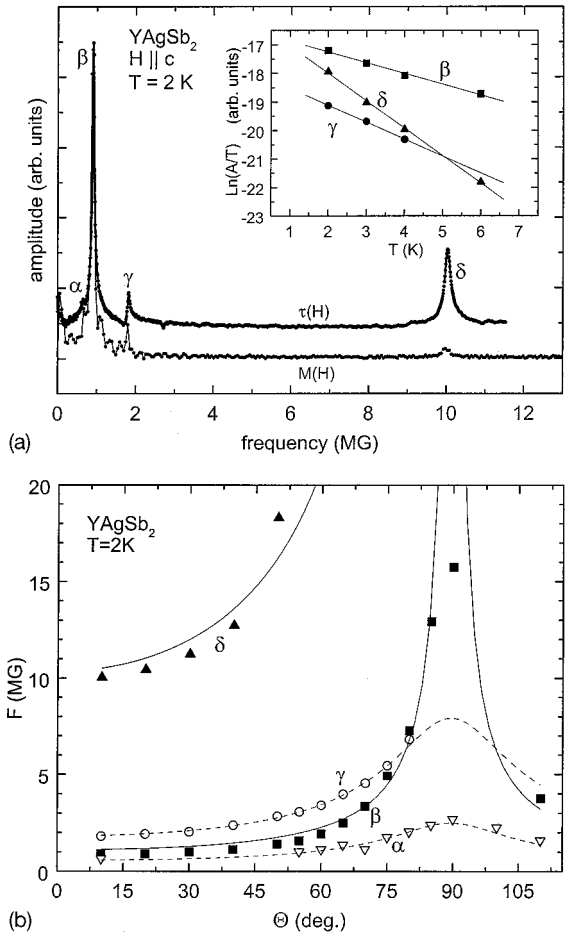

FIG. 2. (a) Fourier spectrum of the oscillations in $YAgSb_2$ for $H \| c$ at 2 K. Inset: Temperature dependence of the amplitudes of the observed oscillations. (b) Angular dependence of the frequencies. θ is relative to the c axis. The lines are fits to the cross-sectional areas of a cylinder (β and δ) and an ellipsoid (α and γ).

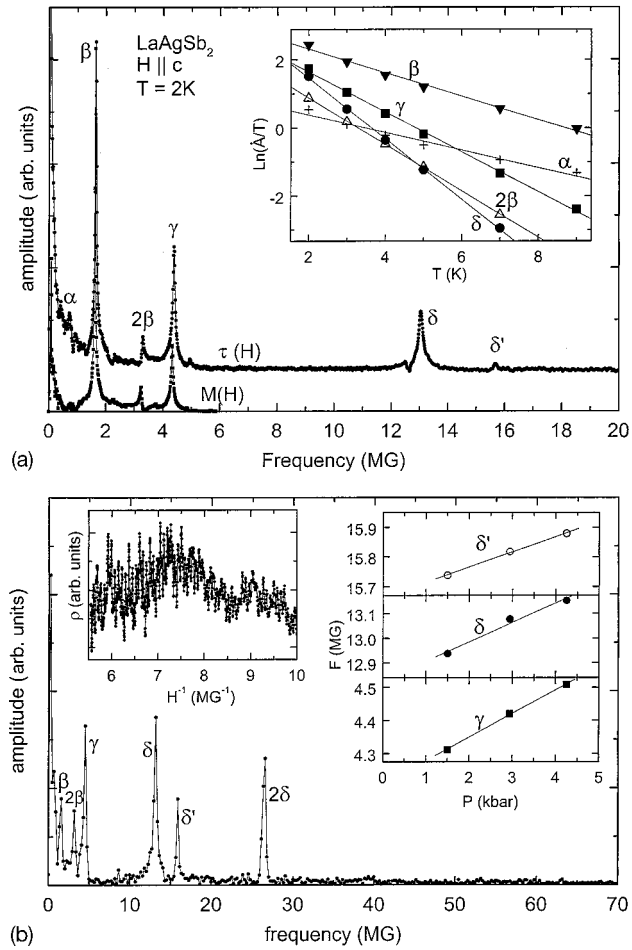

FIG. 3. (a) Fourier spectrum of the oscillations in the torque and magnetization of $LaAgSb_2$ for $H \| c$ at 2 K. Inset: Temperature dependence of the amplitudes of the observed oscillations. (b) Fourier spectra of SdH oscillations in $LaAgSb_2$ at 4.2 kbars and 2.1 K. Left inset: resistivity as a function of inverse field. Right inset: pressure dependence of the frequencies of the observed oscillations.

δ orbits appear to diverge with increasing angle and cannot be fit to the cross section of an ellipsoid with reasonably small c/a ratios. Although the δ orbit is not observed at angles large enough to confirm the shape of the Fermi surface, the angular dependence at low angles is consistent with a cylindrical branch of the Fermi surface, as discussed below. The solid lines in the figure are fits to the angular dependence of the cross sectional area of a cylinder and agree well with the experimental data for both orbits. In all cases, the frequencies, and hence cross sectional areas, are a minimum when the applied field is parallel to the c axis ($\theta=0°$) of the sample. The lack of observed frequencies near $\theta=90°$ may be due to the reduction in amplitude of oscillations in the measured torque near angles with high symmetry, as previously discussed.

$LaAgSb_2$

The field dependence of torque in $LaAgSb_2$ at 2 K and $H \| c$ is more complicated than that observed in $YAgSb_2$. The frequencies of the oscillations are clearly resolved in the FFT [Fig. 3(a)]. Large peaks are present in the spectra at 1.64 MG (β), 4.32 MG (γ), and 12.9 MG (δ). In addition, weak peaks in the FFT indicate the presence of oscillations with frequencies of 0.72 MG (α), 3.22 MG (2β), 4.94 MG (3α), and 15.69 MG (δ'), which becomes clearer in the SdH data shown below. Finally, the δ and δ' orbits likely originate from the same electronic band, discussed later. In the Fourier spectra of the oscillations in the magnetization of $LaAgSb_2$ peaks are present at 0.085 MG (ϕ) and 0.17 MG (2ϕ), which correspond to the low-frequency oscillation and its second harmonic observed in the magnetization as a function of inverse field.

The effective masses, calculated from the temperature dependence of the amplitude of the oscillation [inset Fig. 3(a)], are $m_\beta=0.16(2)m_0$, $m_{2\beta}=0.32(2)m_0$, $m_\gamma=0.28(2)m_0$, and $m_\delta=0.42(2)m_0$. Since the frequency and effective mass of the 2β orbit are twice that of the β orbit, it is concluded that the 2β is the second harmonic of the β orbit. Likewise, the frequency of the 3β orbit suggests that it is the third harmonic of β.

After the removal of the background magnetoresistance, Shubnikov–de Haas oscillations are easily seen in the resistivity as a function of inverse field, which is shown in the left inset of Fig. 3(b). If the frequencies resolved in the FFT of the SdH data [Fig. 3(b)] are extrapolated down to zero pressure, they agree with the dHvA data. The frequencies of the

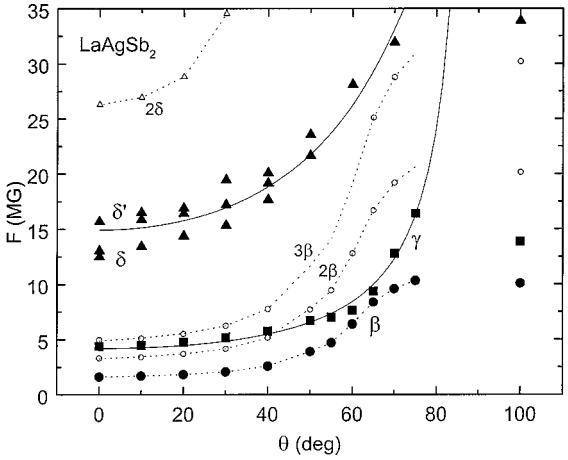

FIG. 4. Angular dependence of the frequencies in $LaAgSb_2$ determined from the FFT of the torque magnetometer data. θ is relative to the c axis. The solid lines are fits to the cross-sectional areas of a cylinder (γ) and an ellipsoid (δ). Dotted lines are guides to the eye.

observed orbits increase approximately linearly with pressure [right inset Fig. 3(b)] with coefficients of 0.07 MG/kbar, 0.08 MG/kbar, and 0.05 MG/kbar for the γ, δ, and δ' orbits, respectively.

The angular dependence of the frequencies of the oscillations in $LaAgSb_2$ (Fig. 4) is similar to that observed in $YAgSb_2$. The frequency corresponding to each of the orbits is minimal for $H \| c$ and increases as the angle increases. The angular dependencies of the β and the δ family of orbits suggest the topologies of these parts of the Fermi surface are primarily ellipsoidal with the major axis parallel to the c axis. The angular dependence of the 2β and 3β orbits is consistent with harmonics of the β orbit. On the other hand, the γ orbit diverges more rapidly as the angle approaches 90°, suggesting a cylindrically shaped section of Fermi surface.

$CeAgSb_2$

Unlike the rest of the series, much higher fields (up to 180 kG) were required to observe SdH oscillations in $CeAgSb_2$. As seen in the resistivity as a function of inverse field for $H \| c$ (Fig. 5), only a single oscillation, with an extremely low frequency ($F \approx 0.25$ MG at 1.2 kbar), is observed in this compound. The frequency of this orbit increases linearly with pressure with a slope of 0.01 MG/kbar. Although the quality of the single crystals of the Ce-containing compounds was comparable to the other samples (residual resistivity ratio≈100), $CeAgSb_2$ manifests complex ferromagnetism (with a possible conical structure) below 9.6 K and a temperature-dependent resistivity typical of a Kondo lattice.[1] These features suggest that the Fermi surface of $CeAgSb_2$ may be substantially different from the other compounds.

$PrAgSb_2$

For $H \| c$ at 2 K, de Haas–van Alphen oscillations were observed, superimposed on the nearly linear magnetic background of $PrAgSb_2$. Due to the much larger response of the magnetic moments to the applied field,[1] the signal to noise

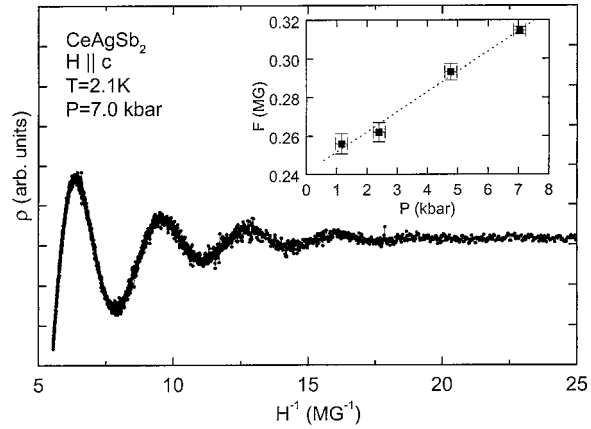

FIG. 5. Shubnikov–de Haas oscillations in $CeAgSb_2$ at 2.1 K and 7.0 kbars. The background magnetoresistance has been removed. Inset: pressure dependence of the SdH oscillation.

ratio of the measurements of the dHvA oscillations suffers in this compound. Despite this significant magnetic background, Fourier analysis of the $M(1/H)$ data reveals three peaks in the spectrum: a strong peak (α) at 0.46 MG, and weak peaks at 0.92 MG (2α) and 1.38 MG (β). The peak in the FFT below the α peak is an artifact of the background subtraction and depends strongly on the method used to remove the contribution from the magnetic sublattice. Since the frequencies of the 2α and β peaks are twice and three times the frequency of the α oscillation, these are possibly harmonics of α. However, the amplitude of the β oscillation is larger than the 2α oscillation, indicating the β oscillation may originate from a different part of the Fermi surface. Unfortunately, the magnitudes of the oscillations are insufficient for a detailed analysis of the temperature dependence of the amplitudes or the angular dependence of the frequencies. Either of these methods would help to resolve the ambiguity of the β component.

$NdAgSb_2$

The amplitudes of the oscillations observed in $NdAgSb_2$ is similar to those observed in $PrAgSb_2$ with an approximate amplitude of $10^{-3}\mu_B$ per formula unit at fields near 50 kG.

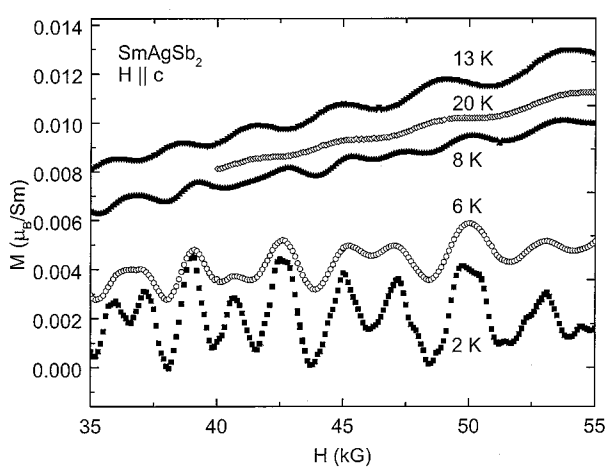

FIG. 6. Magnetization as a function of applied field in $SmAgSb_2$ up to 20 K.

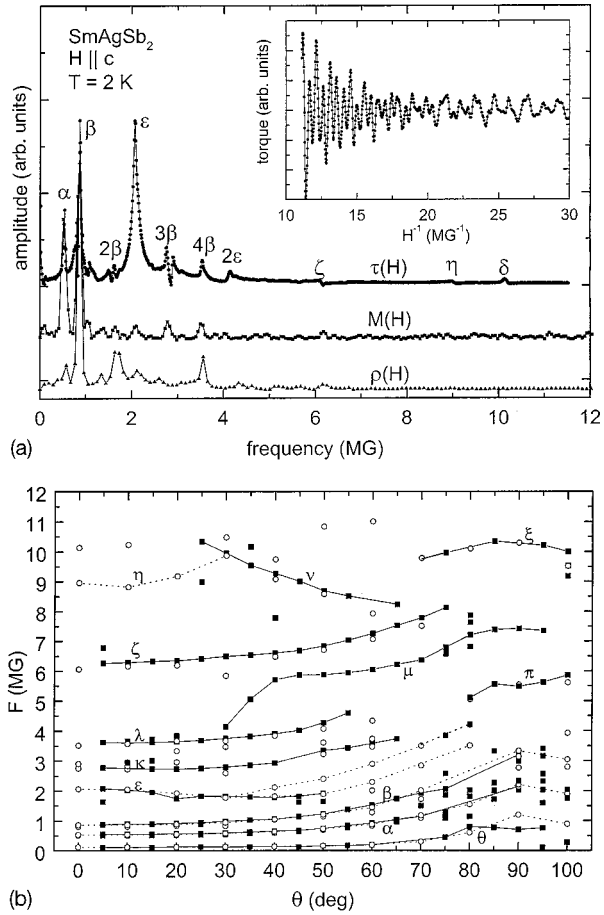

FIG. 7. (a) Fourier spectra of the oscillations in the torque, resistivity, and magnetization of $SmAgSb_2$ for $H \| c$ at 2 K. Inset: Temperature dependence of the amplitudes of the observed oscillations. (b) Angular dependence of the frequencies measured by torque magnetometry (○) and magnetization (■). θ is relative to the c axis. The solid and dotted lines connect the frequencies observed in the torque and magnetization data, respectively.

However, the background magnetization at 2 K for $H \| c$ is only about 20% of that observed in $PrAgSb_2$, creating a more favorable signal to noise ratio. The oscillations are readily observed in $M(1/H)$. Two peaks are visible in the Fourier spectrum indicating the presence of frequencies at 0.56 MG (α) and 1.13 MG (2α). The small maximum in the FFT at very low frequencies changes according to the method of background subtraction and therefore is not likely to originate from a quantum oscillation. The oscillations were of sufficient amplitude to allow an estimation of the effective masses of the electronic bands, through the temperature dependence. Fitting the data to the LK equation yields an effective of the α orbit of 0.07(2) m_0. The effective mass of the 2α peak was found to be 0.17(2) m_0, which is twice the effective mass of the α oscillation within experimental uncertainty and consistent with this oscillation being the second harmonic of the α oscillation.

$SmAgSb_2$

$SmAgSb_2$ is an ideal compound to study the effects of antiferromagnetic ordering on the Fermi surface. The magnetic ordering temperature is large enough ($T_N = 8.8$ K) (Ref. 1) to allow detailed study of the frequencies and their amplitudes in the ordered state. Oscillations are also observed well above T_N, which permits the comparison with the low-temperature data. Furthermore, the single crystals of $SmAgSb_2$ have the smallest residual resistivity of the $RAgSb_2$ series, and hence would be expected to demonstrate quantum oscillations with the largest amplitude. Figure 6 shows these oscillations in the magnetization for $H \| c$ persisting up to temperatures of 20 K. Oscillations in the resistivity are also clearly resolved after the subtraction of the background.

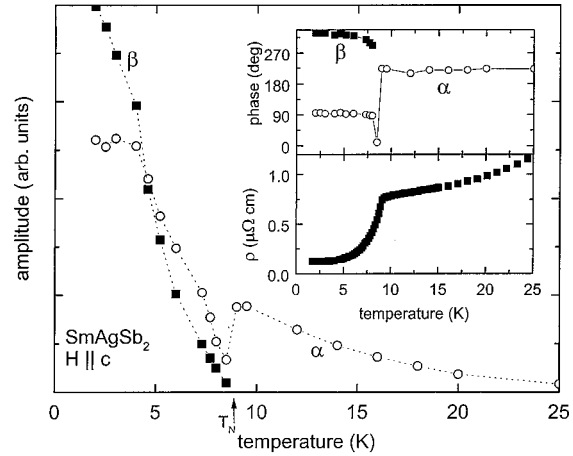

FIG. 8. Temperature dependence of the amplitudes of the α and β oscillations in $SmAgSb_2$. Top inset: temperature dependence of the relative phase of the oscillations. Bottom inset: temperature dependence of the resistivity. Note the suppression of the α amplitude and discontinuity in the phase at $T_N = 8.8$ K.

The spectrum of oscillations observed in $SmAgSb_2$ for $H \| c$ at 2 K [Fig. 7(a)] is much more complicated than those observed in the other members of the series. In the torque data up to 90 kG [inset, Fig. 7 (a)], strong peaks are present at 0.54 MG (α), 0.87 MG (β), and 2.05 MG (ε). Much weaker peaks in the torque data exist at 0.13 MG (θ), 1.62 MG (2β), 2.76 MG (2β), 3.53 MG (4β), 4.14 MG (2ε), 6.17 MG (ζ), 8.97 MG (η), and 10.13 MG (δ). The Fourier spectra of the magnetization and resistivity data up to 55 kG are similar to the FFT of the torque data. However, the ε oscillation is significantly suppressed relative to the other oscillations, in both $M(H)$ and $\rho(H)$, and the α oscillation is weak in $\rho(H)$. The η and δ orbits are not visible in the FFT of either $\rho(H)$ or $M(H)$, probably due to the lower maximum field attainable in the magnetometer.

The observation of additional oscillations in $SmAgSb_2$ may be the result of two different factors. First, the residual resistivity in $SmAgSb_2$ is significantly lower than in the other members of the series. This increases the mean free path of the electrons and allows the higher frequency oscillations to be observed at much lower fields, via a reduction in the Dingle temperature. Second, $SmAgSb_2$ orders antiferromagnetically at 8.8 K, as determined by the temperature-dependent susceptibility[1] and resistivity (bottom inset, Fig. 8). The new periodicity due to the wave vector of antiferromagnetic ordering may significantly perturb the Fermi surface and create new extremal orbits. Unfortunately, the exact nature of the ordered state, such as the wave vector, is not yet

known, which prevents an accurate determination of the electronic band structure in the ordered state.

The angular dependence of the observed frequencies [Fig. 7(b)] is also more complex than any of the other compounds studied here. The frequencies of the α, β, and θ oscillations are minimal at $H \| c$ and increase with increasing angle. None of these frequencies diverge with increasing angle, suggesting the presence of ellipsoidally shaped sections of Fermi surface. Fitting these data to the cross section of an ellipse gives c/a ratios of 4.3, 4.0, and 10.8 for the α, β, and θ oscillations, respectively. The ε, λ, and κ frequencies also appear to be predominately ellipsoidal at low angles. However, these orbits are not observed at large enough angles to accurately determine the topologies of the Fermi surface. The frequency of the ζ oscillation is nearly constant with increasing angle, which indicates the existence of a nearly spherical section of Fermi surface. Finally, additional frequencies, denoted μ, ν, ξ, and π, appear at intermediate angles and manifest complex angular dependencies. It should be noted that for these orbits, in particular, the solid and dotted lines in [Fig. 7(b)] are guides to the eye and only tentatively represent the angular dependence. The origins of these frequencies are currently unknown and are the subject of continuing investigation.

The effect of the magnetic phase transition is particularly evident in the temperature dependence of the amplitude of the oscillations. As seen in Fig. 8, the temperature dependence of the dHvA oscillations for $H \| c$ significantly deviates from monotonically decreasing amplitude with increasing temperature, which is the behavior expected from the Lifshitz-Kosevitch (LK) equation. Instead, an anomalous suppression of the dHvA amplitudes is observed near T_N. Specifically, the amplitude of the α orbit decreases sharply as the temperature approaches T_N. Above T_N, the amplitude partial recovers, and may easily be fit to the LK equation. Fitting this data above T_N yields an effective mass of the α orbit of 0.06(1) m_0, consistent with the rest of the $R\mathrm{AgSb}_2$ series. Likewise, the amplitude of the β orbit (0.87 MG) decreases as the temperature approaches T_N with no observation of this signal above T_N. Below T_N, the fit of the temperature dependence to the LK equation is poor, suggesting that the magnetic ordering is influencing the amplitude. Although the β orbit is only observed below T_N, it is currently impossible to determine whether this is due to a new section of Fermi surface below T_N or increased scattering and broadening of the Fermi surface with increasing temperature. Similar behavior has been previously observed in YbAs (Ref. 11) and SmSb.[12]

As seen in the lower inset of Fig. 8, the resistivity of SmAgSb_2 increases near T_N, due to the introduction of spin-disorder scattering in the paramagnetic state. It is possible that the additional scattering in the paramagnetic state increases the Dingle temperature, and hence suppresses the amplitude. However, if the deviation from the LK behavior were due entirely to the increased scattering from the addition of a magnetic component, it is unlikely that the amplitude of the α oscillation would actually recover immediately above T_N.

When the magnetic sublattice in a compound becomes antiferromagnetically ordered, new periodicity is introduced into the lattice with the wave vector of the magnetic ordering. This extra periodicity may significantly perturb the Fermi surface by rearranging the sections of the Fermi surface and introducing superzone gaps.[13,14] For example, the effect of magnetic ordering on the Fermi surface of rare-earth intermetallic compounds has been previously observed in NdIn_3 which possesses a series of metamagnetic transitions[15] and SmIn_3 which has magnetic transitions at 14.7, 15.2, and 15.9 K.[16] This perturbation of the Fermi surface may be responsible for the appearance of new frequencies below T_N, the phase change, and the anomalous behavior in the amplitude of the α oscillation. However, without explicit knowledge of the ordering wave vector and the band structure of the ordered state, a quantitative analysis of these effects is difficult.

The perturbation of the Fermi surface may account for the temperature dependence of the amplitude in several ways. First, the magnetization M is proportional to $(A'')^{-(1/2)}$, within the LK expression where A'' is the second derivative of the cross sectional area with respect to the wave vector in the direction of the applied field. Increasing this curvature, while keeping the extremal cross-sectional area constant, will diminish the amplitude of the measured oscillation. Second, electron-electron scattering may increase in the magnetically ordered state via an increase in interband scattering between two branches of Fermi surface which are in close proximity in the ordered state. Since no changes in frequency are readily observable for the α oscillation, most likely another, not observed, band is perturbed by the antiferromagnetic ordering and hence indirectly affect the carrier-carrier scattering. This effect would decrease at lower temperatures due to the decrease in thermal broadening of the Fermi surface.

The effect of magnetic ordering may also be seen in a shift in the observed phase of the α oscillation above and below T_N as seen in the $M(1/H)$ data (top inset Fig. 8). Since the frequency of the oscillation is constant, within experimental resolution, above and below the transition, this phase shift may result from the perturbation of the Fermi surface due to a new periodicity arising from the magnetic ordering. The section of Fermi surface would have to altered in such a way that the cross-sectional area remains constant, but the extremal orbit changes from being a minimum to a maximum, or vice versa. This effect may be seen within the LK expression where the relative phase difference between a maximal and minimal orbit is 90°, which is approximately the phase shift observed in the data.

IV. THEORETICAL ANALYSIS

Ab initio local-density approximation (LDA) electronic bands of YAgSb_2 and LaAgSb_2 were calculated using the tight-binding, linear muffin-tin orbital (TB-LMTO) method within the atomic spheres approximation (ASA) developed by Andersen, Jepsen, and Glötzel.[17] Scalar relativistic corrections were included in the calculation and two interstitial spheres were added to make the sum of the volume of the spheres equal to the volume of the tetragonal cell. The $4f$ electrons in Pr, Nd, and Sm are not expected to significantly contribute to the electronic structure near the Fermi energy since these electrons are strongly localized and well screened. Therefore these electrons may be considered part

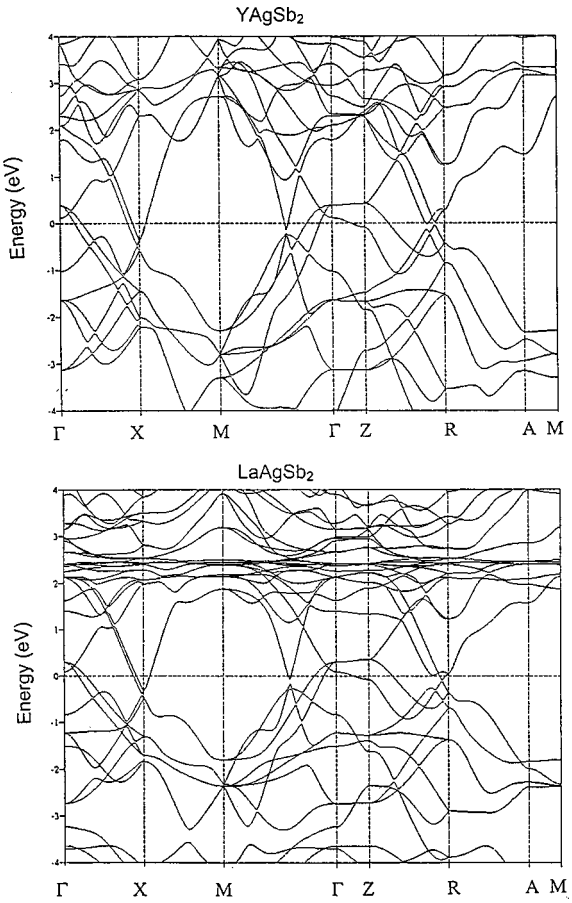

FIG. 9. Band structure of (a) $YAgSb_2$ and (b) $LaAgSb_2$ calculated from tight-binding linear muffin-tin orbital calculations within the atomic spheres approximation.

of the electronic core. This implies that the Fermi surfaces of the rest of the $RAgSb_2$ series in the paramagnetic state are expected to be similar to those obtained for $YAgSb_2$ and $LaAgSb_2$.

Figure 9 shows the electronic structure of $YAgSb_2$ and $LaAgSb_2$ along several high-symmetry directions. Relevant features of these plots include two bands crossing the Fermi energy (E_F) near the Γ point and the two bands crossing E_F near the X point. In addition, another band crosses E_F between Γ and Z. This band is particularly important since it possesses very little curvature, and hence may lead to dramatic changes of the topology of the Fermi surface with small changes in lattice parameters or Fermi energy. Figure 10 shows the Fermi surface of $LaAgSb_2$ in the $k_z=0$ plane of the four bands that cross E_F with the Brillouin zone of a primitive tetragonal lattice displayed in the inset.

Three-dimensional plots of the calculated Fermi surface of $LaAgSb_2$ are shown in Fig. 11. Band 1 is centered at the Γ point and is nearly spherical, with a cross-sectional area in the basal plane corresponding to a frequency of approximately 4.7 MG for $H\|c$. The γ orbit, observed in $SmAgSb_2$ and $LaAgSb_2$ has a frequency of approximately 4.3 MG. In $LaAgSb_2$, the angular dependence of the frequency is nearly constant for low angles, relative to $H\|c$, which is consistent with the calculated band. However, at higher angles, the frequency appears to diverge, indicating nonspherical behavior.

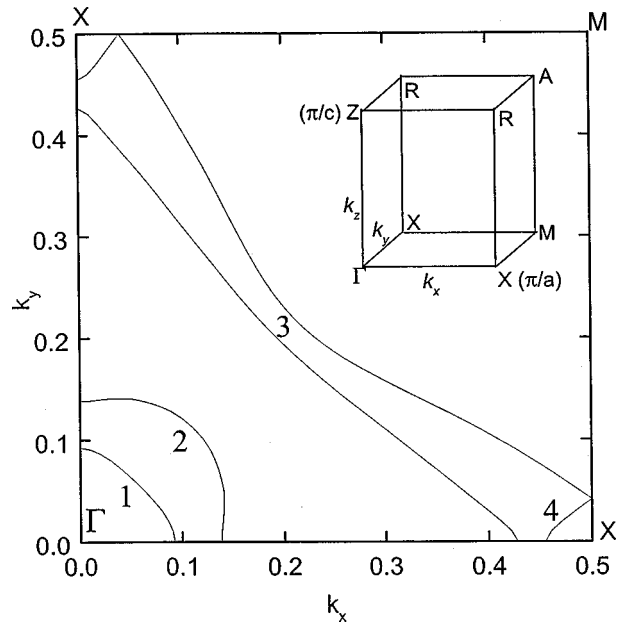

FIG. 10. The Fermi surface of $LaAgSb_2$ in the $k_z=0$ plane, calculated as described in the text. The four bands crossing E_F are labeled 1–4. Inset: the Brillouin zone of a primitive tetragonal lattice with the high-symmetry points labeled.

As seen in Fig. 9, this band is very flat between the Γ and Z points in the zone. If the Fermi energy is increased by a small amount, for example by changing the lattice constants, the topology of this band changes dramatically with the appearance of thin necks connecting this band to the next Brillouin zone. This modified band is now much more consistent with the observed angular dependence of the γ frequencies.

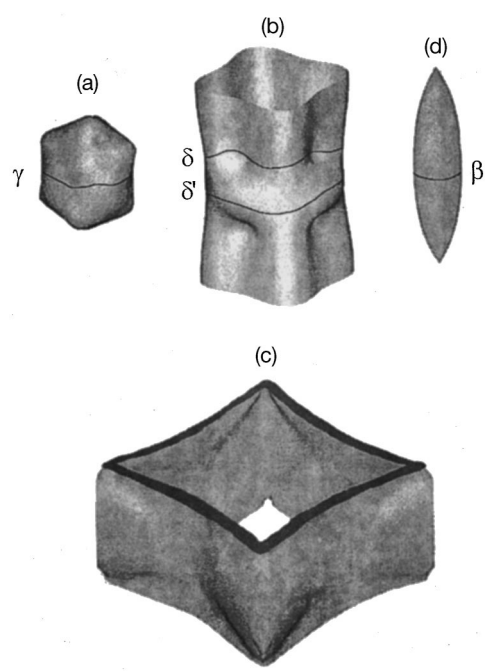

FIG. 11. Three-dimensional plots of the four bands crossing the Fermi surface with the extremal orbits indicated. Bands 1 (a) and 2 (b) are centered at Γ. Band 4 (d) is centered at X. Band 3 (c) extends throughout the zone with the vertices of the squares at the X points.

Although the cross-sectional area for $H \| c$ does not depend strongly on the E_F, this band may also be the origin of the ζ oscillation (6.2 MG) in $SmAgSb_2$ which is nearly spherical. Furthermore, these necks may also help to account for the extremely small frequencies observed for $H \| c$ in most of the compounds. Although the cross sectional area of the necks for $H \| c$ approximately corresponds to the α orbits (0.55 MG) the angular dependence is not in good agreement, since the α orbits appear to be ellipsoidal. Better agreement is found in the θ orbit of $SmAgSb_2$ which has a frequency of 0.13 MG and a shape corresponding to either a cylinder or an elongated ellipsoid with a c/a ratio near 10.

Band 2 is also centered at Γ, but is mostly cylindrical with an axis along k_z, This energy band possesses a nearly circular cross section at $k_z = 0$ and a somewhat square cross section at $k_z = \pi/c$. Maximal cross sectional areas for $H \| c$ correspond to frequencies of 13.2 and 11.5 MG for $k_z = 0$ and π/c, respectively. A minimal area is also observed for $k_z \approx 0.4\pi/c$ with a frequency of 9.7 MG. These frequencies are approximately equal to the δ and δ' frequencies observed in some of the compounds ($F \approx 10.1$ MG for $SmAgSb_2$, 10.04 MG in $YAgSb_2$, and 12.5 MG, 12.9 MG, and 15.7 MG in $LaAgSb_2$). In $SmAgSb_2$ and $YAgSb_2$, the frequency of the δ orbit diverges with increasing angle away from $H \| c$. However, the angular dependence of the δ family of orbits in $LaAgSb_2$ is more closely ellipsoidal than cylindrical. Although the nature of the transition at 210 K (Ref. 1) is currently unknown, a distortion of the lattices may significantly alter the Fermi surface at low temperatures. Taken together, the topology and cross-sectional areas for $H \| c$ suggest that this band is the origin of the δ and δ' orbits observed in the magnetization and torque data. The experimentally determined effective masses of each of the observed frequencies for $H \| c$ are approximately 0.46 m_0 in $YAgSb_2$ and 0.42 m_0 in $LaAgSb_2$.

Band 3 consists of adjacent square cylinders with vertices near each of the X points. One square cylinder is centered at Γ, and the other is centered at the M point. Due to the extremely large cross-sectional areas, it is not expected that any of the features of this band would be visible in the relatively low fields currently accessible. However, it should be noted that at very high fields, the close proximity of these surfaces may result in magnetic breakdown.

An ellipsoidal hole pocket centered at the X point in the Brillouin zone is created by band 4. The cross-sectional area of this band for $H \| c$ ($\theta = 0°$) is maximal at $k_z = 0$ and predicts the presence of a frequency of 0.9 MG. For $H \perp c$ ($\theta = 90°$), the maximal cross-sectional area of this orbit is approximately 3.7 MG, indicating a c/a ratio of about 4. The β frequency is observed in all of the compounds and ranges from 0.86 in $SmAgSb_2$ to 1.64 in $LaAgSb_2$. In each case, the effective masses calculated from the temperature dependence of the amplitudes of the oscillation are approximately 0.17 m_0. The angular dependence of the measured frequencies suggests ellipsoidal topology in $SmAgSb_2$ and $LaAgSb_2$ with a c/a ratio of 4.0. These frequencies and angular dependencies in these compounds are consistent with the calculated dimensions of this energy band centered at the X point. However, in $YAgSb_2$, the frequency of the orbit tends to diverge as the angle increases away from $H \| c$, indicating a more cylindrical topology. Like band 1, a small shift in E_F may cause this band to become more cylindrical and connected by a thin neck to the next Brillouin zone.

Under the application of hydrostatic pressure, the observed frequencies in the SdH data increase in $CeAgSb_2$ and $LaAgSb_2$. It is expected that with sufficient pressure, the FFT spectra of $LaAgSb_2$ would become similar to that of $YAgSb_2$, which has a much smaller rare-earth ion. However, this does not appear to be the case. It is possible that the Fermi surface of $LaAgSb_2$ may be significantly perturbed by the previously mentioned transition near 210 K.[1] Furthermore, the elastic constants may be highly anisotropic, which prevents a direct comparison between the effects of applied pressure and rare earth substitution.

V. CONCLUSION

The $RAgSb_2$ series of compounds is an ideal system for the study of changes in the Fermi surface due to different rare-earth ions and magnetic order. The excellent quality of the crystals allows the measurement of de Haas–van Alphen and Shubnikov–de Haas oscillations at relatively low applied fields and exceptionally high temperatures. The persistence of the oscillations in $SmAgSb_2$ up to temperatures as high as 25 K permits the study of changes in the Fermi surface above and below the ordering temperature. Clearly, significant changes in the Fermi surface of $SmAgSb_2$ result from additional periodicity introduced by magnetic order. Overall, the agreement between the calculated Fermi surface and measured quantum oscillations is good. Although the smaller frequencies are not accounted for in the calculated Fermi surface, the magnitude of many of the frequencies and their angular dependence correlate with the *ab initio* Fermi surface. Knowledge of the Fermi surface in $RAgSb_2$ provides important guidelines for the theoretical explanation of the experimentally observed extremely high anisotropic nonquadratic low-temperature magnetoresistance,[1] as well as may assist in understanding of the magnetic order in these compounds. In addition, high quality samples of $SmAgSb_2$, where the quantum oscillations are observed through the magnetic ordering transition in easily accessible magnetic field/temperature range, are perfect for experimental studies of the effects of magnetic interactions on the wave form of de Haas–van Alphen and Shubnikov–de Haas oscillations.

Neutron or magnetic x-ray diffraction would be useful to determine the microscopic nature of the magnetic ordering in the materials with magnetic rare-earth ions. This knowledge would allow the precise determination of the Fermi surface in the antiferromagnetically ordered states of $SmAgSb_2$. The study of the quantum oscillations at higher fields as well as angle-resolved photoemission and positron annihilation would help resolve larger sections of Fermi surface, not observed in the relatively low fields currently accessible.

ACKNOWLEDGMENTS

Ames Laboratory is operated for the U.S. Department of Energy by Iowa State University under Contract No. W-7405-Eng-82. This work was supported by the Director for Energy Research, Office of Basic Energy Sciences. Work at the National High Magnetic Field Laboratory–Los Alamos National Laboratory was performed under the auspices

of theNational Science Foundation and the U.S. Department of Energy. The pressure cell utilized at the NHMFL-LANL was funded by the National Science Foundation-Division of International Programs in a collaborative project with the Czech Republic. The pressure cell was designed and built by Professor J. Kamarad (Czech Academy of Sciences). S.L.B. appreciates discussions with S. Spagna on the use of the torque magnetometer.

[1] K. D. Myers, S. L. Bud'ko, I. R. Fisher, Z. Islam, H. Kleinke, and P. C. Canfield, J. Magn. Magn. Mater. **205**, 27 (1999).
[2] K. D. Myers, P. C. Canfield, V. A. Kalatsky, and V. L. Pokrovsky, Phys. Rev. B **59**, 1121 (1999).
[3] P. C. Canfield and Z. Fisk, Philos. Mag. B **65**, 1117 (1992).
[4] S. L. Bud'ko, P. C. Canfield, C. H. Mielke, and A. H. Lacerda, Phys. Rev. B **57**, 13 624 (1998).
[5] M. Brylak, M. Möller, and W. Jeitschko, J. Solid State Chem. **115**, 305 (1995).
[6] H. Flandorfer, O. Sologub, C. Godart, K. Hiebl, A. Leithe-Jasper, P. Rogl, and H. Noël, Solid State Commun. **97**, 561 (1996).
[7] Y. Muro, N. Takeda, and M. Ishikawa, J. Alloys Compd. **257**, 23 (1997).
[8] S. Spagna, A. Wilson, M. B. Simmonds, J. Diederichs, and R. E. Sager, Mater. Sci. Forum **302–303**, 401 (1999).
[9] O. Mikulina, A. Syshchenko, V. Sechovsky, H. Nakotte, A. H. Lacerda, and W. P. Beyermann, Bull. Am. Phys. Soc. **44**, 1221 (1999).
[10] D. Shoenberg, *Magnetic Oscillations in Metals* (Cambridge University Press, Cambridge, England, 1984).
[11] N. Takeda, K. Tanaka, M. Kagawa, A. Oyamada, N. Sato, S. Sakatsume, H. Aoki, T. Suzuki, and T. Komatsubara, J. Phys. Soc. Jpn. **62**, 2098 (1993).
[12] K. Tanaka, N. Takeda, Y. S. Kwon, N. Sato, T. Suzuki, and T. Komatsubara, Physica B **186–188**, 150 (1993).
[13] R. J. Elliot and F. A. Wedgewood, Proc. Phys. Soc. London **81**, 846 (1963).
[14] H. Miwa, Prog. Theor. Phys. **29**, 477 (1963).
[15] I. Umehara, T. Ebihara, N. Nagai, K. Satoh, Y. Fujimaki, and Y. Onuki, J. Phys. Soc. Jpn. **61**, 1633 (1992).
[16] T. Ebihara, I. Umehara, A. K. Albessard, Y. Fujimaki, K. Satoh, Y. Onuki, B. Liu, and M. Kasaya, J. Phys. Soc. Jpn. **61**, 2104 (1992).
[17] O. K. Andersen, O. Jepsen, and D. Glötzel, in *Highlights of Condensed-Matter Theory*, edited by F. Bassani, F. Fumi, and M. P. Tosi (Italian Physical Society, Bologne, 1985), pp. 59–176.